ADVANCING EARTH AND SPACE SCIENCE

JGR Space Physics

RESEARCH ARTICLE

10.1029/2021JA029785

Key Points:

- The relationship between the FACs in the magnetotail and the solar wind dynamic pressure is determined for the first time
- The FAC occurrence and density in the magnetotail increase with increasing SW Pdyn, while its footprints ILAT in the polar region decrease
- The response of the FAC to SW Pdyn in the magnetotail has a north-south hemispheric asymmetry

Supporting Information:

Supporting Information may be found in the online version of this article.

Correspondence to:

Z. W. Cheng,
zwcheng@spaceweather.ac.cn

Citation:

Cheng, Z. W., Shi, J. K., Torkar, K., Lu, G. P., Dunlop, M. W., Carr, C. M., et al. (2021). Impact of the solar wind dynamic pressure on the field-aligned currents in the magnetotail: Cluster observation. *Journal of Geophysical Research: Space Physics*, *126*, e2021JA029785. https://doi.org/10.1029/2021JA029785

Received 17 JUL 2021
Accepted 19 NOV 2021

Author Contributions:

Data curation: M. W. Dunlop, C. M. Carr, H. Rème, I. Dandouras
Methodology: K. Torkar, G. P. Lu
Writing – review & editing: Z. W. Cheng, J. K. Shi

Impact of the Solar Wind Dynamic Pressure on the Field-Aligned Currents in the Magnetotail: Cluster Observation

Z. W. Cheng[1], J. K. Shi[1,2], K. Torkar[3], G. P. Lu[4], M. W. Dunlop[5,6], C. M. Carr[7], H. Rème[8], I. Dandouras[8], and A. Fazakerley[9]

[1]State Key Laboratory of Space Weather, NSSC/CAS, Beijing, China, [2]Schools of Astronomy and Space Science, University of Chinese Academy of Sciences, Beijing, China, [3]Space Research Institute, Austrian Academy of Sciences, Graz, Austria, [4]School of Earth and Space Sciences, University of Science and Technology of China, Hefei, China, [5]School of Space and Environment, Beihang University, Beijing, China, [6]Rutherford Appleton Laboratory, Oxfordshire, UK, [7]Blackett Laboratory, Space and Atmospheric Physics Group, Imperial College, London, UK, [8]Institut de Recherche en Astrophysique et Planétologie, Université de Toulouse/CNRS/UPS/CNES, Toulouse, France, [9]MSSL, University College London, London, UK

Abstract We statistically investigate the influence of the solar wind dynamic pressure (SW P_{dyn}) on the field-aligned currents (FACs) in the magnetotail with 1,492 FAC cases from July to October in 2001 and 2004, which covers 74 Cluster crossings of the plasma sheet boundary layer (PSBL) in both storm time and non-storm time. The FAC density in the magnetotail is derived from the magnetic field data with the four-point measurement of Cluster, and the SW P_{dyn} is taken from ACE data. The results indicate the FAC density becomes stronger with increasing SW P_{dyn}. The statistics show that the FAC occurrence increased monotonically with SW P_{dyn} in the three levels (Weak: SW $P_{dyn} < 2$ nPa; Medium: 2 nPa $\leq$ SW $P_{dyn} \leq 5$ nPa; Strong: SW $P_{dyn} > 5$ nPa). The FAC density increased with increasing SW P_{dyn}, while its footprint (invariant latitude, ILAT) in the polar region decreased with increasing SW P_{dyn}. The response of the FAC to SW P_{dyn} in the magnetotail had a north-south hemispheric asymmetry. The FAC density had a better correlation with SW P_{dyn} in the Northern hemisphere, while the footprint had a better correlation with SW P_{dyn} in the Southern hemisphere. Possible underlying mechanisms for our results are analyzed and discussed. However, it requires more observations and simulation studies to find out the mechanism of north-south asymmetry.

1. Introduction

The interplanetary magnetic field (IMF) and the solar wind control physical processes in the magnetosphere, such as magnetic reconnection in the dayside magnetopause and in the magnetotail (Dungey, 1961; Nagai et al., 2005; Nishida, 1983), wave and instability (Hatch et al., 2017; Kavosi & Raeder, 2015; Song et al., 1993), geomagnetic activity (Arnoldy, 1971; Davis et al., 1997; McPherron et al., 1988; Schatten & Wilcox, 1967), as the main effects. The large scale field-aligned current (FAC) plays an important role in transferring the solar wind momentum and energy into the magnetosphere and ionosphere. The FAC is involved in many important physical processes, including magnetic reconnection (Hones, 1979; Ma & Otto, 2013; Scholer & Otto, 1991), field-aligned particle acceleration (Choy et al., 1971; Morooka et al., 2004; Shi et al., 2014), development of the substorm current wedge (Hesse & Birn, 1991; Pytte et al., 1976), and auroral activity (Elphic et al., 1998; Xiong et al., 2014).

In previous studies, many scholars focused on the relationship between the IMF components and the FAC. Based on the ground-based radar and low orbit satellite data, the FACs at low altitude (mainly including Region 1, Region 2, Region 0, and cusp FAC) have been studied in detail. Iijima and Shibaji (1987) found that the dawn-dusk asymmetry of the FACs are caused by the variation of IMF B_y. Yamauchi and Araki (1989) reported that the IMF B_y-dependent cusp region FAC was located around 86–87° invariant latitude (ILAT) near local noon. Taguchi (1992) found that the intensity of the FACs near the midnight auroral oval increased with IMF B_y during northward IMF. The IMF B_z is also an important controlling factor besides the IMF B_y. Papitashvili et al. (2001) provided the distributions of FAC in different IMF B_z conditions. Juusola et al. (2009) found during southward IMF that an increasing FAC intensity corresponded clearly to an increasing $|B_z|$. Gjerloev et al. (2011) found that the nightside FACs showed a clear dependence on IMF B_z.

It was also found that the FACs associated with Joule heating can be affected by the IMF clock angle or cone angle (Li et al., 2011). The field lines along which the nightside field-aligned currents flow are mapped to the magnetospheric tail, thus the FAC observations in the magnetotail also show the IMF dependence. Cheng et al. (2014) found that the IMF B_y played a very important role in controlling the FAC direction. There was a clear north–south hemispheric asymmetry of the polarity of the FACs for both signs of IMF B_y, and this asymmetry of the polarity was more distinct when IMF B_y was positive. Further research showed that the occurrence, density, and the location of the footprint of the FAC were depending on the IMF clock and cone angle (Cheng et al., 2013, 2018).

In fact, besides the IMF components, the solar wind parameters, such as velocity and dynamic pressure are also important controlling factors. Some previous studies have shown that the location of the magnetopause (Shue et al., 1998), geomagnetic pulsations (Chi et al., 1998), the EMIC waves in the magnetosphere (Saikin et al., 2016), the radial distance of the magnetic reconnection site in the magnetotail (Nagai et al., 2005), and geomagnetic D_{st} index (Zhao et al., 2011) have close relationships with solar wind dynamic pressure or velocity. The large scale FAC in the entire solar wind-magnetosphere-ionosphere interaction process should also be influenced by solar wind. The relationship between FAC and si has been studied using data from satellites at low orbit. Iijima and Potemra (1982) investigated the relationship between the Region 1 FAC and SW P_{dyn}. However, they did not examine the Region 2 FAC. Nakano et al. (2009) statistically studied the relationship between the SW P_{dyn} and the intensity of the Region 2 FAC, and they found that Region 2 FAC intensity depends on the SW P_{dyn} during magnetic storms. During non-storm times, however, the correlation is weak. Wang et al. (2006) suggested that the FAC intensity depends on the SW P_{dyn} during storm time. However, they did not distinguish between the Region 1 FAC and the Region 2 FAC. Wing et al. (2011) distinguished between Region 1 and Region 2 FAC, and presented the relationship between the density of FAC and solar wind velocity. It is generally considered that the Region 1 FACs map to the outermost part of magnetotail region, whereas the Region 2 FACs map to regions of the plasma sheet closer to the Earth. The FAC in the magnetotail is connected with that in the polar region through the magnetic field lines (Wild et al., 2004) and it is very important for the magnetosphere-ionosphere coupling which is influenced by solar wind. However, there is no research on the relationship between the magnetotail FAC and SW P_{dyn}, and this paper presents a study on this problem.

In order to investigate the relations between the characteristics of magnetotail FACs and the solar wind, we statistically examined the relationship between the solar wind dynamic pressure and the FAC, as derived from magnetic field measurements by the four Cluster spacecraft. The results show that the SW P_{dyn} has a controlling role on the FAC in the magnetotail. We also discussed the physical mechanism involved.

2. Data and Method

In this study, data of the magnetic field, ions, and electrons, respectively, were taken by the Fluxgate Magnetometer (FGM) (Balogh et al., 1997), the Cluster Ion Spectrometry (CIS) (Rème et al., 2001), and the Plasma Electron And Current Experiment (PEACE) (Johnstone et al., 1997) instruments onboard the Cluster spacecraft. The FAC density can be calculated using magnetic field data from the four Cluster spacecraft by the “curlometer” method (Dunlop et al., 1988). The ion and electron data, combined with the magnetic field data, were used to calculate the plasma β (the ratio of plasma pressure to magnetic pressure). The corresponding IMF, solar wind, and geomagnetic indices (AE, AL, and D_{st}) were obtained from the OMNI database.

Cluster consists of four identical spacecraft that fly in a tetrahedral configuration. The apogee of the four Cluster spacecraft is about 19.6 Earth radii (R_E) and the orbital period is about 57 hr. From July to October in 2001 and 2004, Cluster spends about 60 days crossing the PSBL, and the separation between each Cluster spacecraft was about 2,000 km (1,000 km) in the magnetotail in 2001 (2004). The estimate of the current density inside the volume defined by the tetrahedron relies on the assumption that the magnetic field varies linearly between two spacecraft. When the separation between spacecraft is too large, the linear approximation is not accurate or wrong, and it will be not suitable to use the "Curlometer" method. The small separation satisfies the linear approximation of magnetic field gradient, but we mainly study the large-scale FAC structure in the magnetotail. Therefore, we selected the two years (2001 and 2004) when the separations between two spacecraft were 2,000 km and 1,000 km for analysis. In this case, the separation between two spacecraft is basically equivalent to the scale of FAC in magnetotail. Here we should note that the FAC density calculated by the "Curlometer" method represents the average value.

In general, for studying the FAC in the magnetotail, the search algorithms always choose the FAC case by defining their density and interval, then use the cases to perform statistics and analysis (Cheng et al., 2013; Ohtani

10.1029/2021JA029785

et al., 1988; Shi et al., 2010; Ueno et al., 2002). In this study, the density of FAC case is defined as being larger than 3 pT/km or 2.38 nA/m^2 ($1\ nA/m^2 = 1.26$ pT/km), whereby the current in units of pT/km has been obtained directly from the calculation with the "curlometer" technique. For small FAC density, it will merge into errors or background noise that should not be steady. In this case, we cannot identify the real small FAC density. So we can only study on the FAC case with a big density. In general, researchers have to prescribe a threshold to choose the FAC case to do analysis. Based on the previous magnetotail FAC study (Ohtani et al. (1988) used the minimum limit which the FAC density has been set as 3 mA/m), and combined with the characteristics of FAC density calculated from Cluster data (Shi et al., 2010), the density of a typical FAC density in this study was finally determined to be 3 pT/km. The minimum time interval between two neighboring FAC cases is 5 min. The choice of the 5 min interval is related to the scale of a single FAC case. According to the speed of the Cluster satellite, the distance of the Cluster passing through a FAC sheet is exactly 1,000–2,000 km. Further, if there are two or more FACs with densities above 3 pT/km within 5 min, the largest one was chosen.

In the magnetotail, the FAC mainly exists in the PSBL. We used plasma β to identify the plasma sheet (PS) ($\beta > 1$), PSBL ($0.01 \leq \beta \leq 1$), and the lobe region ($\beta < 0.01$) (Ueno et al., 2002). In order to correlate the IMF and solar wind (64s average data) data to the FAC cases we apply a two-step approach as usual. At first, the time shift between ACE satellite to the average position of dayside magnetopause (10 R_E) is defined as the X component (X_{GSE}) of ACE spacecraft position minus 10 R_E in GSE coordinates, then divided by the magnitude of solar wind speed measured (V_{xGSE}) along the GSE X direction. (Time shift $= (X_{GSE}\text{-}10)/V_{xGSE} \times 106.2 \times (-1)$, in the equation, the unit of X_{GSE} is R_E, the unit of V_{xGSE} is km/s and the unit of Time shift is minute). It is a very simplified approach that may introduce some errors. However, except for extreme excursions in solar wind parameters, the bow shock and magnetopause locations will not move enough to introduce significant uncertainty in the timing of arrival of solar wind structures observed upstream. Secondly, we determine the delay from the average position of dayside magnetopause to the magnetotail. Some authors added a fixed period of time for the inner nightside magnetosphere to respond to the IMF (Cowley & Lockwood, 1992; Østgaard et al., 2005). In order to examine any IMF influence on the inner part of nightside magnetosphere, they have assumed a planar propagation of the solar wind and then added 10 min for the inner nightside magnetosphere to respond to the IMF, the uncertainties of the time shifts are in the range of 0–10 min (Collier et al., 1998; Østgaard et al., 2005). The effect of the solar wind interaction to the magnetopause will be quickly propagate to the magnetotail. In most FAC cases, the time shift could be roughly considered as 0. In a few FAC cases, SW P_{dyn} showed some fluctuations within $a \pm 5$ min interval. To combine the location and scale of the FAC, the maximum time shift is no more than 5 min. In addition, we used the International Geomagnetic Reference Field (IGRF) model (internal) and the Tsyganenko 96 (T96) model (external) (Tsyganenko & Stern, 1996) to trace all FAC cases along the magnetic field lines from the magnetotail to the polar ionosphere, and obtained the ILAT and the magnetic local time (MLT).

Figure 1 shows the FAC cases with their corresponding SW P_{dyn} when the Cluster spacecraft were crossing the PSBL in the magnetotail. The top panel of Figure 1 shows a typical example that occurred in non-storm time on 17 July 2001. The bottom panel of Figure 1 shows an example that occurred in storm time on 17 August 2001. The black dotted line denotes the time shift that the IMF from ACE observation influence on the magnetotail, the blue line denotes the solar wind dynamic pressure and the black line denotes the density of FACs. We did not distinguish between the earthward FAC and tailward FAC. On 17 July 2001, from 06:30 UT to 08:40 UT, Cluster detected a total of 12 FAC cases. In this period, the minimum value of D_{st} was only −18 nT, and the maximum value of AE was 184 nT. The D_{st} values indicate that no storm occurred. The SW P_{dyn} was also weak, the maximum value was only about 2.3 nPa. However, the top panel of Figure 1 shows clearly that the variation of FAC density was well correlated with the SW P_{dyn}. On 17 August 2001, a strong storm occurred with the minimum D_{st} value of −105 nT. The maximum value of AE was more than 1,000 nT and we confirmed that a substorm had happened at that time. Cluster crossed the PSBL from the sudden commencement to the early main phase of the storm (09:00 UT to 15:40 UT) and detected a total of 16 FAC cases. From the bottom panel of Figure 1 we can see that both the SW P_{dyn} and FAC density show a strong disturbance, the maximum value of SW P_{dyn} is more than 15 nPa and the maximum FAC density is about 17 nA/m^2, the trend of FAC density was consistent with the SW P_{dyn}. Figure 1 just shows typical example cases in storm time and non-storm time. Based on this idea, we performed a statistical analysis of the relationship between the FAC cases and SW P_{dyn}.

According to the selection criteria mentioned above, 1,492 FAC cases in the magnetotail were selected during Cluster crossings from July to October in 2001 and 2004. All the FAC cases were distributed in 74 times of

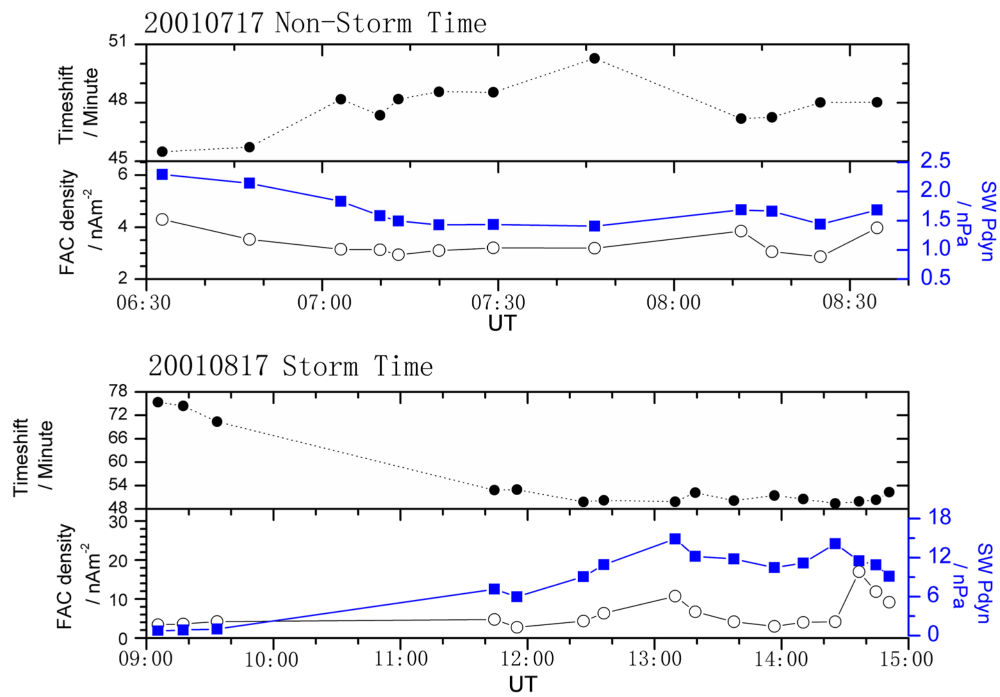

Figure 1. Two examples of the field-aligned current (FAC) cases with their corresponding solar wind dynamic pressure (SW P_{dyn}) when the Cluster spacecraft were crossing the PSBL in the magnetotail in non-storm time (the top panel) and storm time (the bottom panel), respectively. The black dotted line denotes the time shift that the interplanetary magnetic field (IMF) from ACE observation influence on the magnetotail, the blue line denotes the solar wind dynamic pressure and the black line denotes the density of FACs.

plasma sheet crossing (37 times in 2001 and 2004, respectively). The number of FAC cases observed during each crossing were different, from several to dozens. Then we matched the SW P_{dyn} to every FAC case and mapped it along the field line to the polar region at altitude of 100 km. Thereafter we performed a statistical analysis on the FAC occurrence, density, and footprint as functions of SW P_{dyn}.

3. Statistical Results

3.1. The Relationship Between the Frequency of Occurrence of FAC and SW P_{dyn}

The selected 1,492 FAC cases include tailward and earthward FAC ones, as well as northern and southern hemispheric cases. Left two panels in Figure 2 show the distributions of 1,492 FAC cases in the magnetotail in the *X–Y* plane (top) and *X–Z* plane (bottom) in the GSM coordinate system and the right panel shows the distribution of their mapping footprints in the polar region. The Tsyganenko T96 model is used for mapping. The red points denote the earthward FACs and the blue points denote the tailward ones. The locations of the FAC cases are limited within Y_{GSM} from $-15\ R_E$ to $15\ R_E$ (~4 hr MLT around midnight). From Figure 2 we can see that the FAC cases and footprints seem to distribute uniformly in the magnetotail (*X–Y* or *X–Z* plane in the GSM coordinate) and in the polar region, respectively. The results of a detailed analysis will be shown later.

The relationship between the occurrence of FAC and SW P_{dyn} was studied first. The top panel of Figure 3 shows the number of FAC cases (black circles) and total time of the observation (blue squares) under the three different SW P_{dyn} levels (Weak: SW P_{dyn} < 2 nPa; Medium: 2 nPa ≤ SW P_{dyn} ≤ 5 nPa; Strong: SW P_{dyn} > 5 nPa). The bottom panel of Figure 3 shows the normalized occurrence (black squares) with the three P_{dyn} levels. When SW P_{dyn} < 2 nPa, the total observation time (During the period of plasma sheet crossing) was 100,850 min and 746 FAC cases were observed. Here we define the occurrence as the ratio of the number of FAC cases to the total observation time (i.e., 746/100,850 ≈ 7.40×10^{-3}/ min). When 2 nPa ≤ SW P_{dyn} ≤5 nPa, the total observation time was 65,392 min and 620 FAC cases were observed, and the occurrence was about 9.48×10^{-3}/ min. When SW P_{dyn} > 5 nP, the total observation time was 11,335 min and 126 FAC cases were observed, and the occurrence

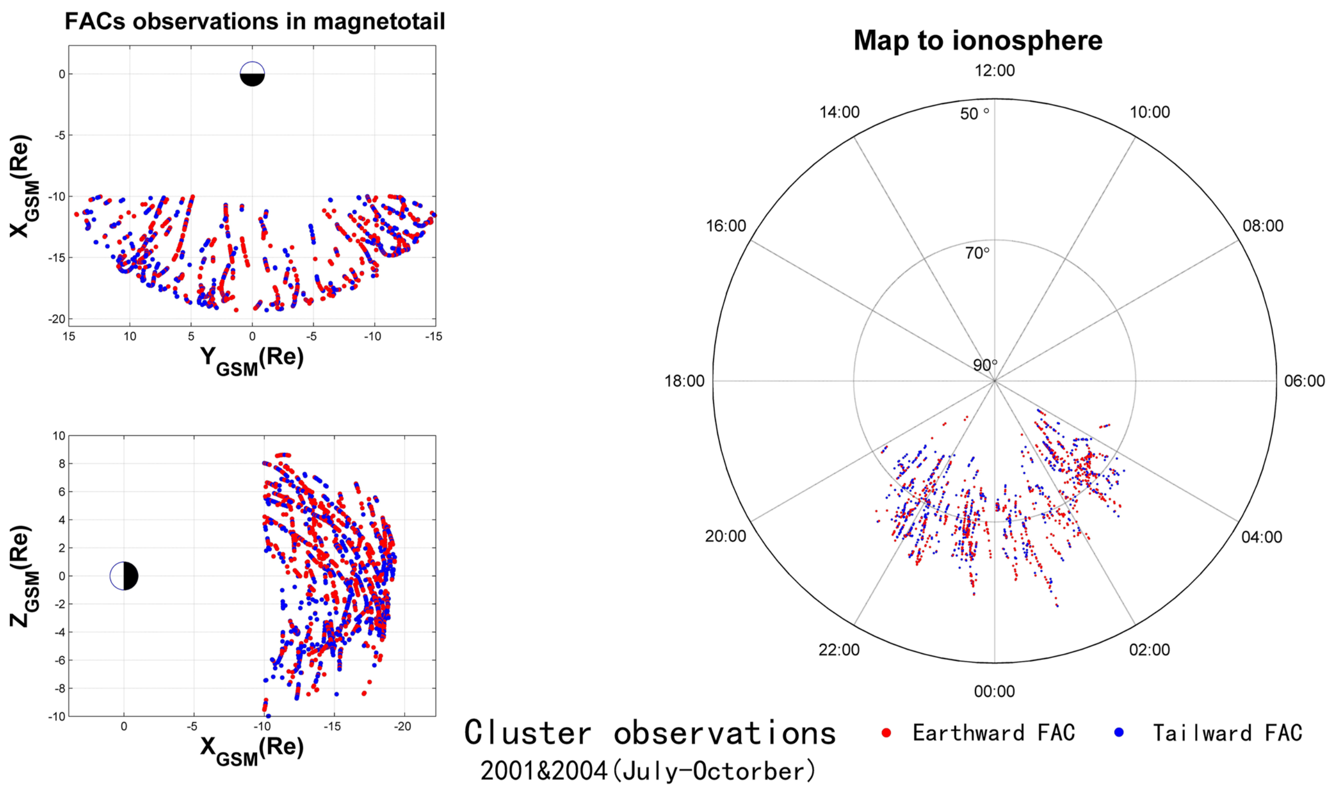

Figure 2. Distribution of the field-aligned current (FAC) cases in the magnetotail (left two panels) in the GSM *X–Y* plane (top) and *X–Z* plane (bottom) and the distribution of footprints in the polar region (right panel). The red points denote the earthward and the blue points the tailward FACs.

was about 11.11×10^{-3}/ min. For comparison purposes, the occurrences were normalized and they were 26.4%, 33.9% and 39.7%, respectively.

From the top panel of Figure 3 we can see that the number of FAC cases were 746, 620, and 126 under weak, medium, and strong SW P_{dyn} levels, respectively. The number of FAC cases decreased with an increasing SW P_{dyn}. It is because the higher the SW P_{dyn} is, the shorter the total observation time will be. However, we can see from the bottom panel of Figure 3 that the FAC occurrence increases monotonically with SW P_{dyn}. This means that the higher the SW P_{dyn} is, the more easily the FACs occur.

3.2. The Relations Between the FAC Density and Footprint Location and SW P_{dyn}

Figure 4 shows the mean density (black dots) and the mean ILAT of the footprints (white squares) of FAC cases in each of the three SW P_{dyn} levels. The standard deviation of the mean (error bar) is given. The numbers beside the dots and squares are the numbers of FAC cases. We can see that the FAC density increased with increasing SW P_{dyn}, while the ILAT of its footprint in the polar region decreased with increasing SW P_{dyn}. This indicates that strong FACs were more common at lower ILAT. The slope from level 2 (i.e., 2 nPa ≤ SW P_{dyn} ≤ 5 nPa) to level 3 (i.e., SW P_{dyn} > 5 nPa) is bigger than that from level 1 (i.e., SW P_{dyn} < 2 nPa) to level 2, which shows that the magnitude of the variation of the FAC density and its footprint ILAT are increasing. This means that the stronger the SW P_{dyn} was, the greater its role in controlling the FAC.

Furthermore, we calculated some parameters of FAC cases in each of the three SW P_{dyn} levels, including the FAC density and ILAT of FAC footprint mean values, median values, standard errors (SE), standard deviations (SD), and the ranges (maximum–minimum), as shown in Table 1. We can see that the density median value increased with increasing SW P_{dyn}, which is consistent with the variation of the mean value. The ILAT median value decreased with increasing SW P_{dyn}, which is also consistent with the variation of the mean value. SD shows how widely scattered the FAC cases are, and it also increases with increasing SW P_{dyn}. The increase of SE was mainly

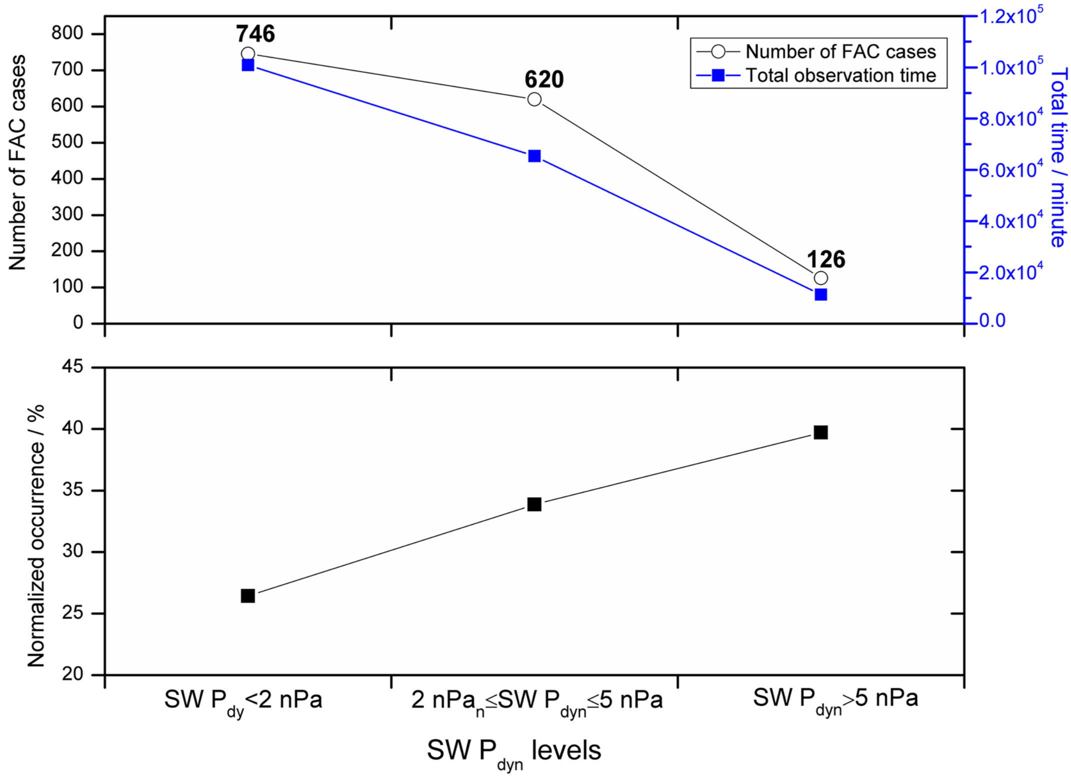

Figure 3. (top) The number of field-aligned current (FAC) cases (circles) and total time of the observation (blue squares) under three different solar wind dynamic pressure (SW P_{dyn}) levels (Weak: SW P_{dyn} < 2 nPa; Medium: 2 nPa ≤ SW P_{dyn} ≤ 5 nPa; Strong: SW P_{dyn} > 5 nPa). (bottom) The normalized occurrence (black squares) with the three SW P_{dyn} levels.

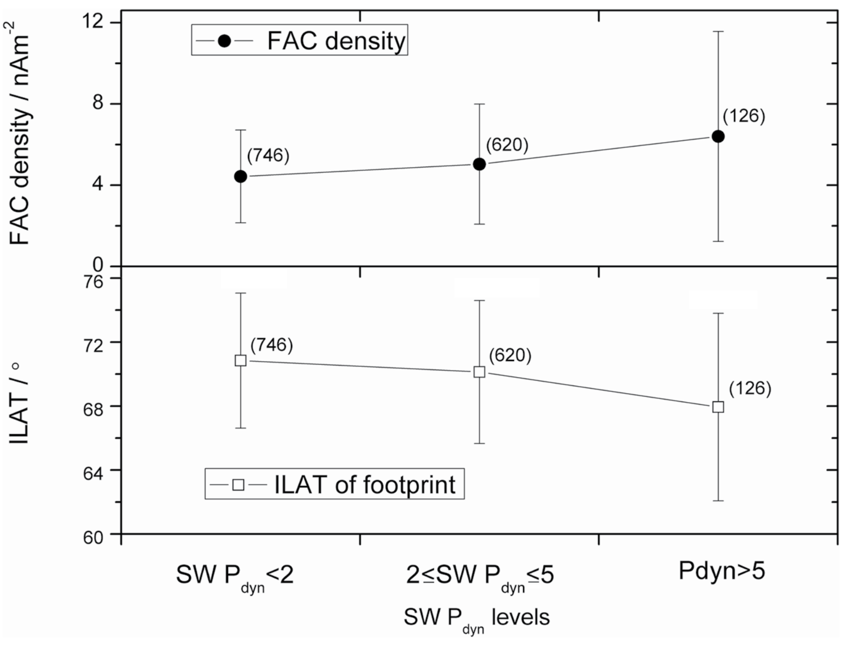

Figure 4. (top) Mean density (black dots) and standard deviation of the field-aligned current (FAC) cases in each solar wind dynamic pressure (SW P_{dyn}) level. (bottom) Mean ILAT (white squares) and standard deviation of the footprint of the FAC cases in each SW P_{dyn} level. The numbers beside the dots and squares are the numbers of FAC cases.

 10.1029/2021JA029785

Table 1
Some Parameters of the FAC Cases in the Three SW P_{dyn} Levels

SW P_{dyn} level	FAC case number	FAC density (nA/m^2)				
		Mean	Median	SE	SD	FAC density range (max–min)
Weak	746	4.4	3.6	0.08	2.3	16.6
Medium	620	5.0	4.2	0.12	2.9	25.7
Strong	126	6.4	4.6	0.46	5.1	33.9

SW P_{dyn} level	FAC case number	FAC footprint (ILAT/°)				
		Mean	Median	SE	SD	ILAT range (Max–Min)
Weak	746	70.8	70.6	0.15	4.2	20.4
Medium	620	70.1	69.8	0.18	4.5	24.0
Strong	126	67.9	67.5	0.52	5.9	21.9

Note. Here: Weak, SW P_{dyn} < 2 nPa; Medium, 2 nPa ≤ SW P_{dyn} ≤ 5 nPa; Strong, SW P_{dyn} > 5 nPa. Standard errors (SE) of the mean FAC density and the mean ILAT, standard deviations (SD) of the mean FAC density and the mean ILAT. (Please note that SE equals SD divided by square root of the number of FAC cases).

due to the decrease of the number of FAC cases with increasing SW P_{dyn}. In addition, the FAC density range increased with increasing SW P_{dyn}.

Figure 5 shows the mean density (black squares) and SD of FAC cases as a function of SW P_{dyn}. The bin width of SW P_{dyn} is 1 nPa. Pressures above 8 nPa are treated as a single bin because of the small number of FAC cases. The number beside the black square is the number of FAC cases. From Figure 5 we can see that even if the statistic interval becomes small, it has the same trend as that in Figure 4. The number of FAC cases rapidly decreases when the SW P_{dyn} is larger than 4 nPa, especially in the range 7 nPa ≤ SW P_{dyn} < 8 nPa, the number of FAC cases is only 12.

One of the purposes of setting the three SW P_{dyn} levels in this paper is to ensure that there are enough cases in every statistical interval to distinguish between the northern and southern hemisphere. Figure 6 is the same as Figure 4, but for different hemispheres (the left panel [a] is for the northern and the right [b] is for the southern

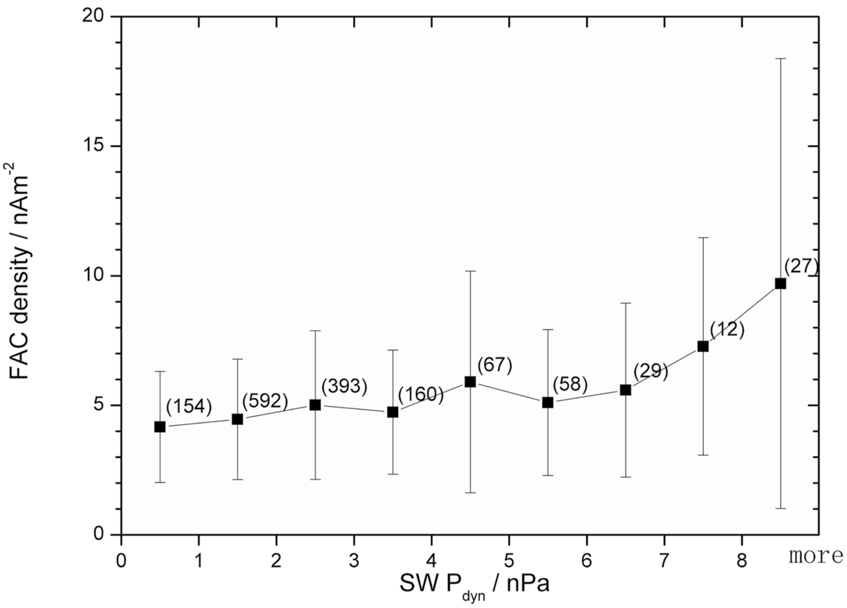

Figure 5. The mean density (black squares) and standard deviation (SD) of field-aligned current (FAC) cases as a function of solar wind dynamic pressure (SW P_{dyn}). The bin width of SW P_{dyn} is 1 nPa. Pressures above 8 nPa are treated as a single bin because of the small number of FAC cases. The number beside the black square is the number of FAC cases.

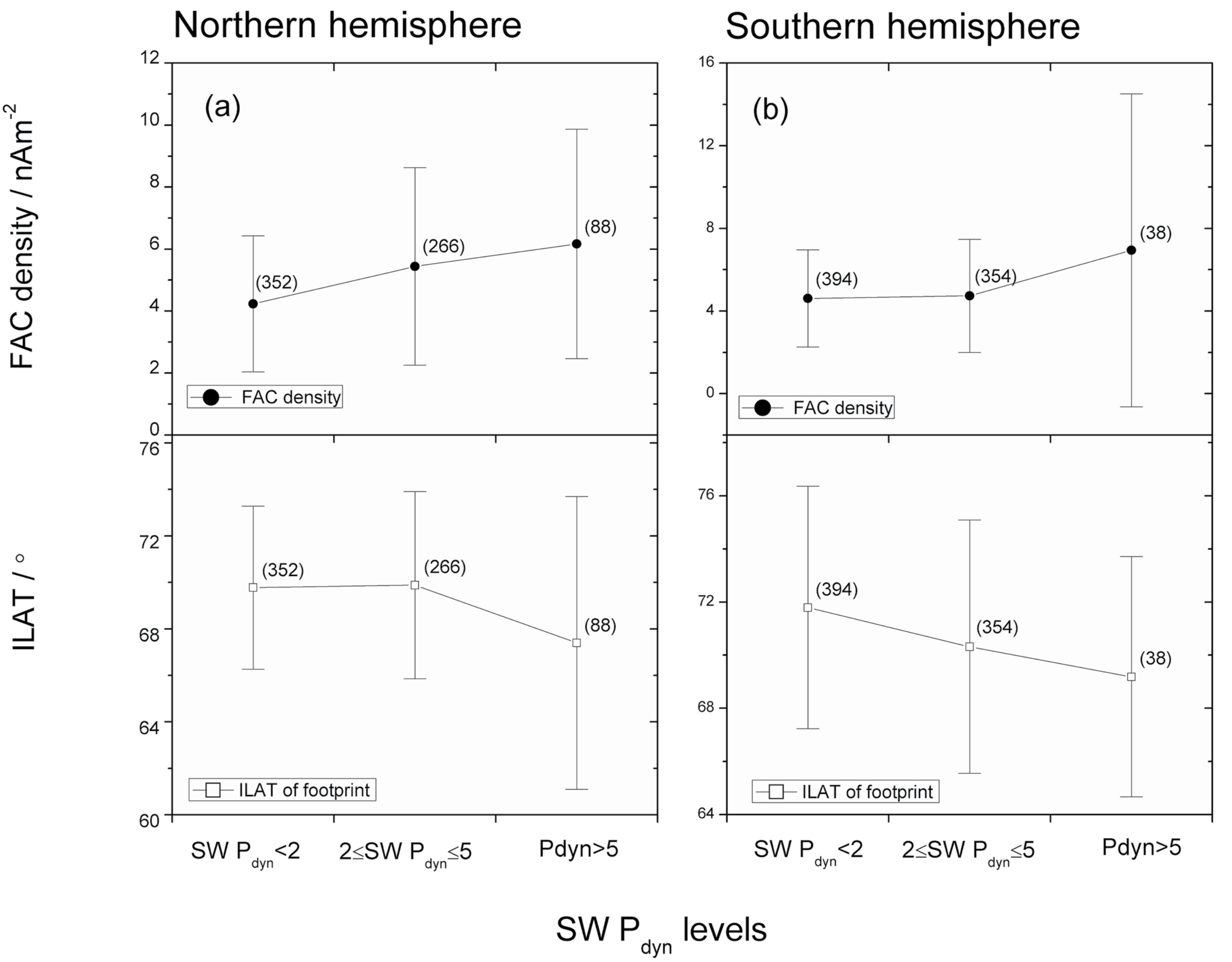

Figure 6. Same as Figure 4, but for different hemispheres (the left panel [a] is for the northern and the right [b] is for the southern one). The numbers beside the dots and squares are the numbers of field-aligned current (FAC) cases.

one). The numbers beside the dots and squares are the numbers of FAC cases. In the northern (southern) hemisphere, the numbers of FAC cases were 352 (394), 266 (354), and 88 (38) under weak, medium, and strong SW P_{dyn} levels, respectively. We can see that in the northern hemisphere the FAC density increased with the three SW P_{dyn} levels, while in the southern one the FAC density had a significant enhancement only under strong SW P_{dyn} conditions. However, in the southern hemisphere the ILAT of the footprints increased with all three SW P_{dyn} levels, while in the northern one the ILAT of the footprints had a significant enhancement only under strong SW P_{dyn} conditions. The maximum/minimum FAC density and ILAT in the southern hemisphere were larger than those in the northern one. These results suggest that the FAC density in the magnetotail and its footprint in the polar region response to SW P_{dyn} have a north-south asymmetry.

4. Discussion

In this study we investigated the FAC density in the PSBL in the magnetotail. Indeed, some authors have studied the FAC density in the low altitude Region 1 vs. MLT (Iijima & Potemra, 1978). Here, we compare our results with previously published results. Figure 7 shows the MLT distribution of the magnetotail FAC density (black circles) in the condition SW $P_{dyn} < 2$ (our result with Cluster observations) and the result of low altitude Region 1 FAC in the condition $|AL| \geq 100$ nT by Iijima and Potemra based on Triad observations (blue squares). From Figure 7 we can see that the variations of FAC density at different altitudes have the same tendency. This can

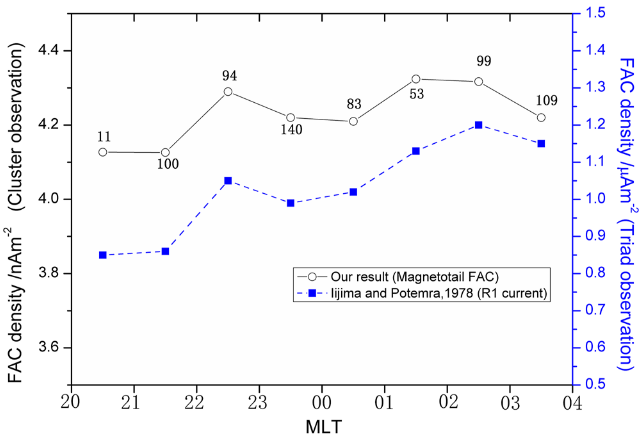

Figure 7. The magnetic local time (MLT) distribution of the magnetotail field-aligned current (FAC) density in the condition SW P_{dyn} < 2 nPa (black circles), and the result of low altitude (Region 1) FAC density in the condition |AL| ≥ 100 nT by Iijima and Potemra (blue squares) based on Triad observations.

be understood as a signature of the FACs in the PSBL being connected with those in the polar region through the magnetic field lines.

The FAC cases under the condition |AL| < 100 nT were only a small part of all cases in our study, so it had little effect on the result. From Figure 7, we also can see that the FAC density on the dawnside is slightly larger than that on the duskside. The maximum value of FAC density is about 4.32 nA/m^2 in the region 1 ≤ MLT < 2, and the minimum value is about 4.13 nA/m^2 in the region 21 ≤ MLT < 22. The difference between maximum and minimum is only 0.19 nA/m^2, not exceeding 5% of the minimum value. For correlating the FAC density with the SW P_{dyn}, the MLT influence could be ignored.

Our results indicate that the FAC in the magnetotail is affected by the solar wind dynamic pressure. This manifests itself in three aspects: (a) In the three SW P_{dyn} levels, the FAC occurrence increases monotonically with SW P_{dyn}; (b) The FAC density increases with increasing SW P_{dyn}; (c) The FAC footprint (ILAT) in the polar region decreases with increasing SW P_{dyn}. When the solar wind dynamic pressure increases, the magnetosphere shrinks. Previous observations and simulations have suggested that the location of the subsolar magnetopause depends approximately on the balance between the solar wind dynamic pressure and the magnetospheric magnetic pressure (Martyn, 1951; Shue et al., 1997), and the spatial distribution of the magnetic pressure in the magnetosphere varies with the solar wind dynamic pressure. Some studies have proven that the low altitude Region 1 and Region 2 FAC are generated by magnetospheric pressure (e.g., Nakano et al., 2009; Yang et al., 1994). Because FAC in the magnetotail links to FAC at low altitude, we can therefore expect that the FAC in the magnetotail would depend on the solar wind dynamic pressure.

Some studies have suggested that the solar wind conditions determine the efficiency and location of reconnection at the dayside magnetopause, which in turn determines the efficiency of solar wind-magnetospheric coupling (e.g., Boudouridis et al., 2004; Nagai et al., 2005). An increase in reconnection efficiency can cause an intensification of the magnetospheric convection potential and, hence, the FAC density (Korth et al., 2010). The solar wind dynamic pressure strongly affects dayside reconnection as well as polar-cap convection, and also enhances magnetotail reconnection and magnetospheric convection (Boudouridis et al., 2007). On the basis of former research, The mechanisms of SW P_{dyn} 's impact on the FAC boil down to two major points: Firstly, the spatial distribution of the magnetic pressure in the magnetosphere varies with the SW P_{dyn}, and the FACs are closely related with the magnetic pressure; secondly, the SW P_{dyn} enhancement can increase reconnection and solar wind–magnetosphere coupling efficiency (increased cross-polar cap potential and enhanced ionospheric convection), the occurrence and density of FAC would vary as well. So the solar wind dynamic pressure is an important factor which affected the occurrence and density of the FAC in the magnetotail.

In addition, the solar wind dynamic pressure modifies the location of FAC footprints, which has already been confirmed for Region 1 FAC at low altitude (Wing et al., 2011). Since Region 1 FACs and magnetotail FACs connect together and are closely related with the location of the boundary between open and closed magnetic flux, an increasing SW P_{dyn} compresses the magnetic field inside the magnetosphere, and the footprints of the magnetic lines along which the FACs move to lower latitudes. Therefore the magnetotail FAC footprint location must follow the expansion to lower latitudes as well. Conversely, when the SW P_{dyn} decreases, the footprints of magnetic field lines and the FACs move to poleward.

Our results also show that the FAC in the magnetotail controlled by SW P_{dyn} has a north-south asymmetry. The causes of the asymmetry are complex, there are several possible causes. The first reason may be due to the configuration of the magnetosphere, as we know the geomagnetic dipole tilt angle makes the influence of solar wind on the magnetosphere asymmetrical in the northern and southern hemisphere, so this leads to the FAC in the magnetotail has a north-south hemispheric asymmetry. The second reason is the conductivity in the ionosphere (Fujii et al., 1981; Ohtani et al., 2005; Vallat et al., 2005) which also relates to geomagnetic dipole tilt angle. The amount and distribution of ionospheric conductivity can be changed by solar EUV radiation in two hemispheres. Different hemispheres differently receive solar EUV radiation in different amounts. Research has shown that the high latitude field-aligned intensities increased by a factor of 1.5–1.8 in the summer polar cap in comparison with the winter hemisphere (Christiansen et al., 2002), so related FAC both in ionosphere and magnetosphere also have a north-south asymmetry. In addition, Christiansen et al. (2002) found the seasonal dependence in the global FAC system is generated and maintained by the various solar wind-magnetosphere interaction processes, such as the quasi-viscous interaction and reconnection. This argument could also be used to interpret the north-south asymmetry of FAC. It requires more observations and simulation studies to pinpoint underlying physical mechanisms for such asymmetry.

5. Summary

We used four Cluster spacecraft magnetic field data from July to October in 2001 and 2004 to calculate the FAC density. 1,492 FAC cases were selected for analysis. The occurrence, density, and the location of footprints of the FAC response in the magnetotail to the SW P_{dyn} have been studied in detail. Our results show that: (a) The number of FAC cases decreases with increasing SW P_{dyn}, however the FAC occurrence increases monotonically with SW P_{dyn}. (b) The FAC density increases with increasing SW P_{dyn}, while its footprint (ILAT) in the polar region decreases with increasing SW P_{dyn}. (c) The FAC controlled by SW P_{dyn} has a north-south asymmetry. The FAC density has a close correlation with SW P_{dyn} in the northern hemisphere rather than in the southern hemisphere. Conversely, the footprint location has a good correlation with SW P_{dyn} in the southern hemisphere rather than the northern hemisphere. (d) Comparing the MLT distribution (around midnight) of the magnetotail FAC density with the result of low altitude Region 1 FAC, the density variations of FACs with MLT at low altitude and in the magnetotail have the same tendency. This implies that the FACs in the magnetotail are associated with the FACs in the polar region. We also studied the influence of the MLT on the density distribution of FAC, and found that the MLT influence on the correlation between the density distribution and SW P_{dyn} could be ignored.

The impact of solar wind dynamic pressure on the FACs in the magnetotail is presented for the first time, and the results are very important for understanding the solar wind-magnetosphere-ionosphere coupling. Although we discussed some possible mechanisms for the magnetotail FACs response to the SW P_{dyn}, the multiple control mechanisms involved in the process of the FAC variation need to be studied further.

Data Availability Statement

The authors thank the Cluster team for their data and software (https://cosmos.esa.int/web/csa).

Acknowledgments
This work was supported by National Natural Science Foundation of China (41874172 and 42074201), the Specialized Research Fund for State Key Laboratories, the International Partnership Program of Chinese Academy of Sciences (183311KYSB20200003), Pandeng Program of National Space Science Center, Chinese Academy of Sciences, and the Chinese Meridian Project. IMF, solar wind, and geomagnetic indices were obtained from the GSFC/SPDF OMNIWeb interface at http://omniweb.gsfc.nasa.gov.

References

Arnoldy, R. L. (1971). Signature in the interplanetary medium for substorms. *Journal of Geophysical Research*, *76*(22), 5189–5201. https://doi.org/10.1029/ja076i022p05189

Balogh, A., Carr, C. M., Acuña, M. H., Dunlop, M. W., Beek, T. J., Brown, P., et al. (1997). The cluster magnetic field investigation. *Space Science Reviews*, *19*(10/12), 1207–1217. https://doi.org/10.5194/angeo-19-1207-2001

Boudouridis, A., Lyons, L. R., Zesta, E., & Ruohoniemi, J. M. (2007). Dayside reconnection enhancement resulting from a solar wind dynamic pressure increase. *Journal of Geophysical Research*, *112*, A06201. https://doi.org/10.1029/2006ja012141

Boudouridis, A., Zesta, E., Lyons, L. R., Anderson, P. C., & Lummerzheim, D. (2004). Magnetospheric reconnection driven by solar wind pressure fronts. *Annales Geophysicae*, *22*, 1367–1378. https://doi.org/10.5194/angeo-22-1367-2004

Cheng, Z. W., Shi, J. K., Dunlop, M., & Liu, Z. X. (2013). Infuences of the interplanetary magnetic eld clock angle and cone angle on the eld-aligned currents in the magnetotail. *Geophysical Research Letters*, *40*, 5355–5359. https://doi.org/10.1002/2013GL056737

Cheng, Z. W., Shi, J. K., Dunlop, M., & Liu, Z. X. (2014). IMF By-controlled field-aligned currents in the magnetotail during northward interplanetary magnetic field. *Journal of Atmospheric and Solar-Terrestrial Physics*, *115–116*, 52–58. https://doi.org/10.1016/j.jastp.2013.11.003

Cheng, Z. W., Shi, J. K., Zhang, J. C., Torkar, K., Kistler, L. M., Dunlop, M., et al. (2018). Influence of the IMF cone angle on invariant latitudes of polar region footprints of FACs in the magnetotail: Cluster observation. *Journal of Geophysical Research: Space Physics*, *123*, 2588–2597. https://doi.org/10.1002/2017JA024941

Chi, P. J., Russell, C. T., Bloom, R. M., & Singer, H. J. (1998). Solar wind control of ultralow-frequency wave activity at L=3. *Journal of Geophysical Research*, *103*, 29467–29477. https://doi.org/10.1029/98JA02161

Choy, L. W., Arnoldy, R. L., Potter, W., Kintner, P., & Cahill, L. J., Jr. (1971). Field-aligned particle currents near an auroral arc. *Journal of Geophysical Research*, *76*(34), 8279–8298. https://doi.org/10.1029/ja076i034p08279

Christiansen, F., Papitashvili, V. O., & Neubert, T. (2002). Seasonal variations of high latitude field-aligned currents inferred from Ørsted and Magsat observations. *Journal of Geophysical Research*, *107*(A2), 1029. https://doi.org/10.1029/2001JA900104

Collier, M. R., Slavin, J. A., Lepping, R. P., Szabo, A., & Ogilvie, K. (1998). Timing accuracy for the simple planar propagation magnetic eld structures in the solar wind. *Geophysical Research Letters*, *25*, 2509–2512. https://doi.org/10.1029/98gl00735

Cowley, S. W. H., & Lockwood, M. (1992). Excitation and decay of solar wind-driven ows in the magnetosphere–ionosphere system. *Annales Geophysicae*, *10*, 103–115.

Davis, C. J., Wild, M. N., Lockwood, M., & Tulunay, Y. K. (1997). Ionospheric and geomagnetic response to changes in IMF Bz: A super-posed epoch study. *Annales Geophysicae*, *15*, 217–230. https://doi.org/10.1007/s005850050435

Dungey, J. W. (1961). Interplanetary magnetic field and the auroral zone. *Physical Review Letters*, *6*, 47–48. https://doi.org/10.1103/physrevlett.6.47

Dunlop, M. W., Southwood, D. J., Glassmeier, K.-H., & Neubauer, F. M. (1988). Analysis of multipoint magnetometer data. *Advances in Space Research*, *8*(9–10), 273–277. https://doi.org/10.1016/0273-1177(88)90141-x

Elphic, R. C., Bonnell, J. W., Strangeway, R. J., Kepko, L., Ergun, R. E., McFadden, J. P., et al. (1998). The auroral current circuit and field-aligned currents observed by FAST. *Geophysical Research Letters*, *25*(12), 2033–2036. https://doi.org/10.1029/98GL01158

Fujii, R., Iijima, T., Potemra, T. A., & Sugiura, M. (1981). Seasonal dependence of large-scale birkeland currents. *Geophysical Research Letters*, *8*(10), 1105–1106. https://doi.org/10.1029/gl008i010p01103

Gjerloev, J. W., Ohtani, S., Iijima, T., Anderson, B., Slavin, J., & Le, G. (2011). Characteristics of the terrestrial field-aligned current system. *Annales Geophysicae*, *29*, 1713–1729. https://doi.org/10.5194/angeo-29-1713-2011

Hatch, S. M., LaBelle, J., Lotko, W., Chaston, C. C., & Zhang, B. (2017). IMF control of Alfvénic energy transport and deposition at high latitudes. *Journal of Geophysical Research: Space Physics*, *122*, 12189–12211. https://doi.org/10.1002/2017JA024175

Hesse, M., & Birn, J. (1991). On depolarization and its relation to the substorm current wedge. *Journal of Geophysical Research*, *96*(A11), 19417–19426. https://doi.org/10.1029/91JA01953

Hones, E. W. (1979). Transient phenomena in the magnetotail and their relation to substroms. *Space Science Reviews*, *23*(3), 393–410. https://doi.org/10.1007/bf00172247

Iijima, T., & Potemra, T. A. (1978). Large-scale characteristics of field-aligned currents associated with substorms. *Journal of Geophysical Research*, *83*, 599–615. https://doi.org/10.1029/JA083iA02p00599

Iijima, T., & Potemra, T. A. (1982). The relationship between interplanetary quantities and Birkeland current densities. *Geophysical Research Letters*, *9*, 442–445. https://doi.org/10.1029/gl009i004p00442

Iijima, T., & Shibaji, T. (1987). Global characteristics of northward IMF associated (NBZ) field-aligned currents. *Journal of Geophysical Research*, *92*, 2408–2424. https://doi.org/10.1029/JA092iA03p02408

Johnstone, A. D., Alsop, C., Burge, S., Carter, P. J., Coker, A. J., Fazakerley, A. N., et al. (1997). Peace: A plasma electron and current experiment. *Space Science Reviews*, *79*(1/2), 351–398. https://doi.org/10.1023/A:1004938001388

Juusola, L., Kauristie, K., Amm, O., & Ritter, P. (2009). Statistical dependence of auroral ionospheric currents on solar wind and geomagnetic parameters from 5 years of CHAMP satellite data. *Annales Geophysicae*, *27*, 1005–1017. https://doi.org/10.5194/angeo-27-1005-2009

Kavosi, S., & Raeder, J. (2015). Ubiquity of Kelvin–Helmholtz waves at Earth's magnetopause. *Nature Communications*, *6*(1), 7019. https://doi.org/10.1038/ncomms8019

Korth, H., Anderson, B. J., & Waters, C. L. (2010). Statistical analysis of the dependence of large-scale Birkeland currents on solar wind parameters. *Annales Geophysicae*, *28*(2), 515–530. https://doi.org/10.5194/angeo-28-515-2010

Li, W., Knipp, D., Lei, J., & Raeder, J. (2011). The relation between dayside local Poynting ux enhancement and cusp reconnection. *Journal of Geophysical Research*, *116*, A08301. https://doi.org/10.1029/2011JA016566

Ma, X., & Otto, A. (2013). Mechanisms of field-aligned current formation in magnetic reconnection. *Journal of Geophysical Research*, *118*, 4906–4914. https://doi.org/10.1002/jgra.50457

Martyn, D. F. (1951). The theory of magnetic storms and auroras. *Nature*, *167*, 92–94. https://doi.org/10.1038/167092a0

McPherron, R. L., Baker, D. N., Bargatze, L. F., Clauer, C. R., & Holzer, R. E. (1988). IMF control of geomagnetic activity. *Advances in Space Research*, *8*(9–10), 71–86. https://doi.org/10.1016/0273-1177(88)90114-7

Morooka, M., Mukai, T., & Fukunishi, H. (2004). Current-voltage relationship in the auroral particle acceleration region. *Annales Geophysicae*, *22*(10), 3641–3655. https://doi.org/10.5194/angeo-22-3641-2004

Nagai, T., Fujimoto, M., Nakamura, R., Baumjohann, W., Ieda, A., Shinohara, I., et al. (2005). Solar wind control of the radial distance of the magnetic reconnection site in the magnetotail. *Journal of Geophysical Research*, *110*, A09208. https://doi.org/10.1029/2005JA011207

Nakano, S., Ueno, G., Ohtani, S., & Higuchi, T. (2009). Impact of the solar wind dynamic pressure on the Region 2 field-aligned currents. *Journal of Geophysical Research*, *114*, A02221. https://doi.org/10.1029/2008JA013674

Nishida, A. (1983). IMF control of the Earth's Magnetosphere. In J. G. Roederer (Ed.), *Progress in solar-terrestrial physics* (pp. 185–200). Springer. https://doi.org/10.1007/978-94-009-7096-0_14

Ohtani, S., Kokubun, S., Elphic, R. C., & Russell, C. T. (1988). Field-aligned current signatures in the near-tail region: 1.ISEE observations in the plasma sheet boundary layer. *Journal of Geophysical Research*, *93*(A9), 9709–9720. https://doi.org/10.1029/JA093iA09p09709

Ohtani, S., Ueno, G., Higuchi, T., & Kawano, H. (2005). Annual and semiannual variations of the location and intensity of large-scale field-aligned currents. *Journal of Geophysical Research*, *110*, A01216. https://doi.org/10.1029/2004JA010634

Østgaard, N., Tsyganenko, N. A., Mende, S. B., Frey, H. U., Immel, T. J., Fillingim, M., et al. (2005). Observations and model predictions of substorm auroral asymmetries in the conjugate hemispheres. *Geophysical Research Letters*, *32*, L05111. https://doi.org/10.1029/2004GL022166

Papitashvili, V. O., Christiansen, F., & Neubert, T. (2001). Field-aligned currents during IMF ∼0. *Geophysical Research Letters*, *28*, 3055–3058. https://doi.org/10.1029/2001gl012944

Pytte, T., McPherron, R. L., & Kokubun, S. (1976). The ground signatures of the expansion phase during multiple onset substorms. *Planetary and Space Science*, *24*, 1115–1132. https://doi.org/10.1016/0032-0633(76)90149-5

Rème, H., Aoustin, C., Bosqued, J. M., Dandouras, I., Lavraud, B., Sauvaud, J. A., et al. (2001). First multispacecraft ion measurements in and near the Earth's magnetosphere with the identical Cluster ion spectrometry (CIS) experiment. *Annales de Geophysique*, *19*(10/12), 1303–1354. https://doi.org/10.5194/angeo-19-1303-2001

Saikin, A. A., Zhang, J.-C., Smith, C. W., Spence, H. E., Torbert, R. B., & Kletzing, C. A. (2016). The dependence on geomagnetic conditions and solar wind dynamic pressure of the spatial distributions of EMIC waves observed by the Van Allen Probes. *Journal of Geophysical Research: Space Physics*, *121*, 4362–4377. https://doi.org/10.1002/2016ja022523

Schatten, K. H., & Wilcox, J. W. (1967). Response of geomagnetic activity index Kp to interplanetary magnetic eld. *Journal of Geophysical Research*, *72*(21), 5185–5191. https://doi.org/10.1029/jz072i021p05185

Scholer, M., & Otto, A. (1991). Magnetotail reconnection: Current diversion and field-aligned currents. *Geophysical Research Letters*, *18*(4), 733–736. https://doi.org/10.1029/91GL00361

Shi, J. K., Cheng, Z. W., Zhang, T. L., Dunlop, M., Liu, Z. X., Torkar, K., et al. (2010). South-north asymmetry of field-aligned currents in the magnetotail observed by Cluster. *Journal of Geophysical Research*, *115*, A07228. https://doi.org/10.1029/2009JA014446

Shi, J. K., Zhang, Z., Torkar, K., Dunlop, M., Fazakerley, A., Cheng, Z., et al. (2014). Temporal and spatial scales of a high-flux electron disturbance in the cusp region: Cluster observations. *Journal of Geophysical Research: Space Physics*, *119*, 4536–4543. https://doi.org/10.1002/2013JA019560

Shue, J.-H., Chao, J. K., Fu, H. C., Russell, C. T., Song, P., Khurana, K. K., et al. (1997). A new functional form to study the solar wind control of the magnetopause size and shape. *Journal of Geophysical Research*, *102*(A5), 9497–9511. https://doi.org/10.1029/97JA00196

Shue, J.-H., Song, P., Russell, C. T., Steinberg, J. T., Chao, J. K., Zastenker, G., et al. (1998). Magnetopause location under extreme solar wind conditions. *Journal of Geophysical Research*, *103*(A8), 17691–17700. https://doi.org/10.1029/98JA01103

Song, P., Russell, C. T., Strangeway, R. J., Wygant, J. R., Cattell, C. A., Fitzenreiter, R. J., et al. (1993). Wave properties near the subsolar magnetopause: Pc 3- 4 energy coupling for northward interplanetary magnetic field. *Journal of Geophysical Research*, *98*, 187–196. https://doi.org/10.1029/92ja01534

Taguchi, S. (1992). By-controlled eld-aligned currents near midnight auroral oval during northward interplanetary magnetic eld. *Journal of Geophysical Research*, *97*(A8), 12231–12243. https://doi.org/10.1029/92ja00548

Tsyganenko, N. A., & Stern, D. P. (1996). Modeling the global magnetic field of the large-scale Birkeland current systems. *Journal of Geophysical Research*, *101*, 27187–27198. https://doi.org/10.1029/96JA02735

Ueno, G., Ohtani, S., Saito, Y., & Mukai, T. (2002). Field-aligned currents in the outermost plasma sheet boundary layer with Geotail observation. *Journal of Geophysical Research*, *107*, 1399. https://doi.org/10.1029/2002JA009367

Vallat, C., Dandouras, I., Dunlop, M., Balogh, A., Lucek, E., Parks, G. K., et al. (2005). First current density measurements in the ring current region using simultaneous multispacecraft Cluster FGM data. *Annales Geophysicae*, *23*, 1849–1865. https://doi.org/10.5194/angeo-23-1849-2005

Wang, H., Lühr, H., Ma, S. Y., Weygand, J., Skoug, R. M., & Yin, F. (2006). Field-aligned currents observed by CHAMP during the intense 2003 geomagnetic storm events. *Annales Geophysicae*, *24*, 311–324. https://doi.org/10.5194/angeo-24-311-2006

Wild, J. A., Milan, S. E., Owen, C. J., Bosqued, J. M., Lester, M., Wright, D. M., et al. (2004). The location of the open-closed magnetic field line boundary in the dawn sector auroral ionosphere. *Annales Geophysicae*, *22*, 3625–3639. https://doi.org/10.5194/angeo-22-3625-2004

Wing, S., Ohtani, S., Johnson, J. R., Echim, M., Newell, P. T., Higuchi, T., et al. (2011). Solar wind driving of dayside field-aligned currents. *Journal of Geophysical Research*, *116*, A08208. https://doi.org/10.1029/2011JA016579

Xiong, C., LührWang, H. H., Johnsen, M. G., & Johnsen, M. G. (2014). Determining the boundaries of the auroral oval from CHAMP field-aligned current signatures-Part 1. *Annales Geophysicae*, *32*, 609–622. https://doi.org/10.5194/angeo-32-609-2014

Yamauchi, M., & Araki, T. (1989). The interplanetary magnetic field *By*-dependent field-aligned current in the dayside polar cap under quiet conditions. *Journal of Geophysical Research*, *94*, 2684–2690. https://doi.org/10.1029/JA094iA03p02684

Yang, Y. S., Spiro, R. W., & Wolf, R. A. (1994). Generation of region 1 current by magnetospheric pressure gradients. *Journal of Geophysical Research*, *99*(A1), 223–234. https://doi.org/10.1029/93JA02364

Zhao, H., Zong, Q. G., Wei, Y., & Wang, Y. F. (2011). Influence of solar wind dynamic pressure on geomagnetic Dst index during various magnetic storms. *Science China Technological Sciences*, *54*, 1445–1454. https://doi.org/10.1007/s11431-011-4319-y